Supplement of Atmos. Chem. Phys., 23, 1147–1167, 2023
https://doi.org/10.5194/acp-23-1147-2023-supplement

Atmospheric Chemistry and Physics Open Access

Supplement of

Measurement report: Intensive biomass burning emissions and rapid nitrate formation drive severe haze formation in the Sichuan Basin, China – insights from aerosol mass spectrometry

Zhier Bao et al.

Correspondence to: Yang Chen (chenyang@cigit.ac.cn)

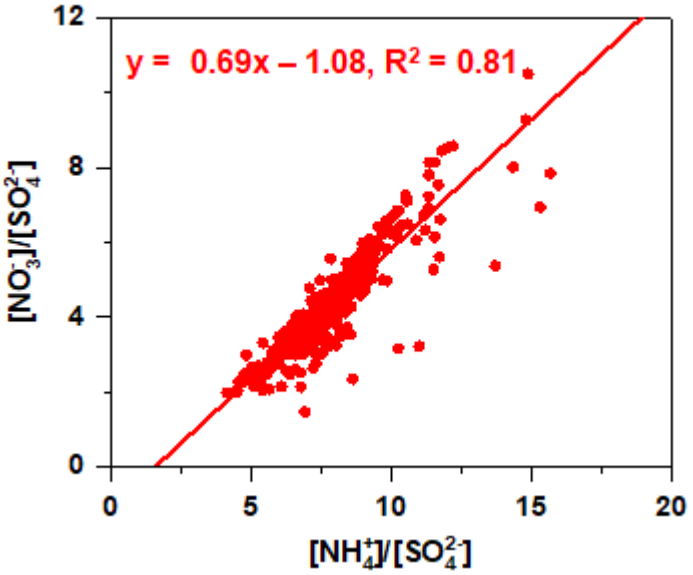

Fig. S1 Molar ratios of nitrate to sulphate vs. ammonium to sulphate during daytime

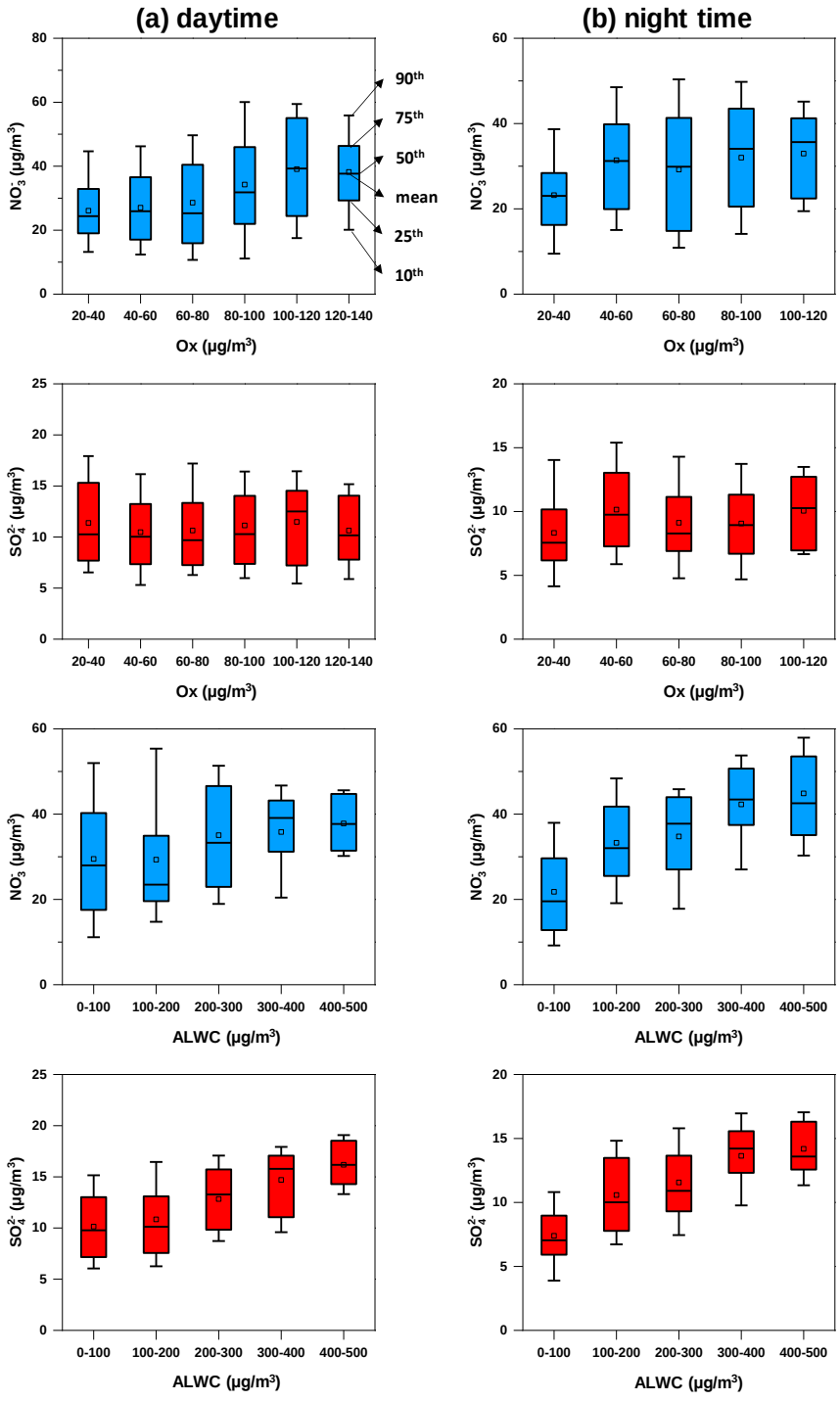

Fig. S2 Variation of nitrate and sulphate as Ox/ALWC increases during (a) daytime (left column) and (b) nighttime (right column). The data of nitrate and sulphate concentrations were grouped into different bins according to 20 μg/m^3 increment of Ox, and 100 μg/m^3 increment of ALWC. The mean (square), 50th (horizontal line inside the box), 25th and 75th percentiles (lower and upper box), and 10th and 90th percentiles (lower and upper whiskers) of the box chart are marked in (a).

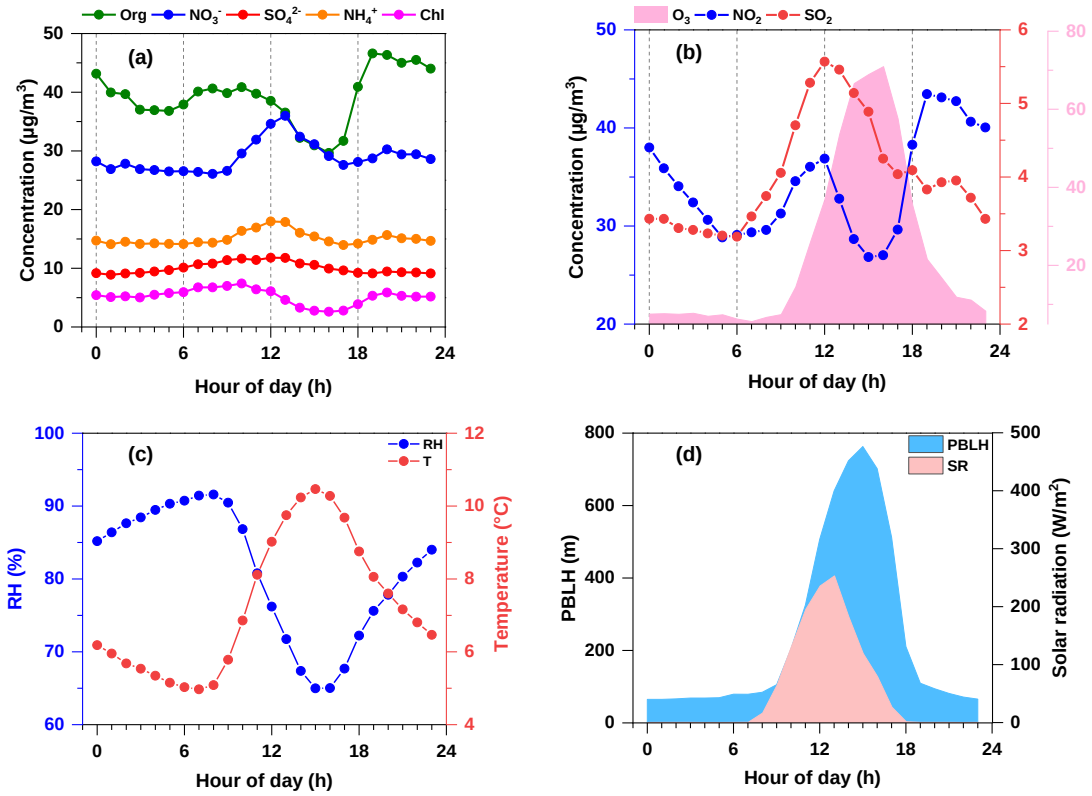

Fig. S3 Diurnal variations of (a) chemical composition in NR-$PM_{2.5}$, (b) O_3, NO_2, and SO_2, (c) RH and temperature, (d) planet boundary layer height (PBLH) and solar radiation (SR). The PBLH was derived from the European Centre for Medium-Range Weather Forecasts (ECMWF) dataset of ERA5 hourly data (https://cds.climate.copernicus.eu/cdsapp#!/home).

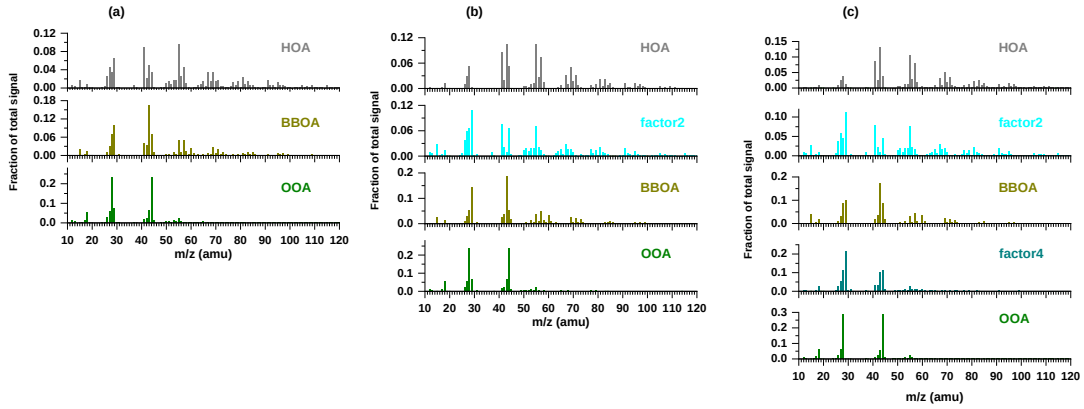

Fig. S4 Mass spectrum profile of OA factors resolved by PMF for (a) 3-, (b) 4-, and (c) 5-factor solutions

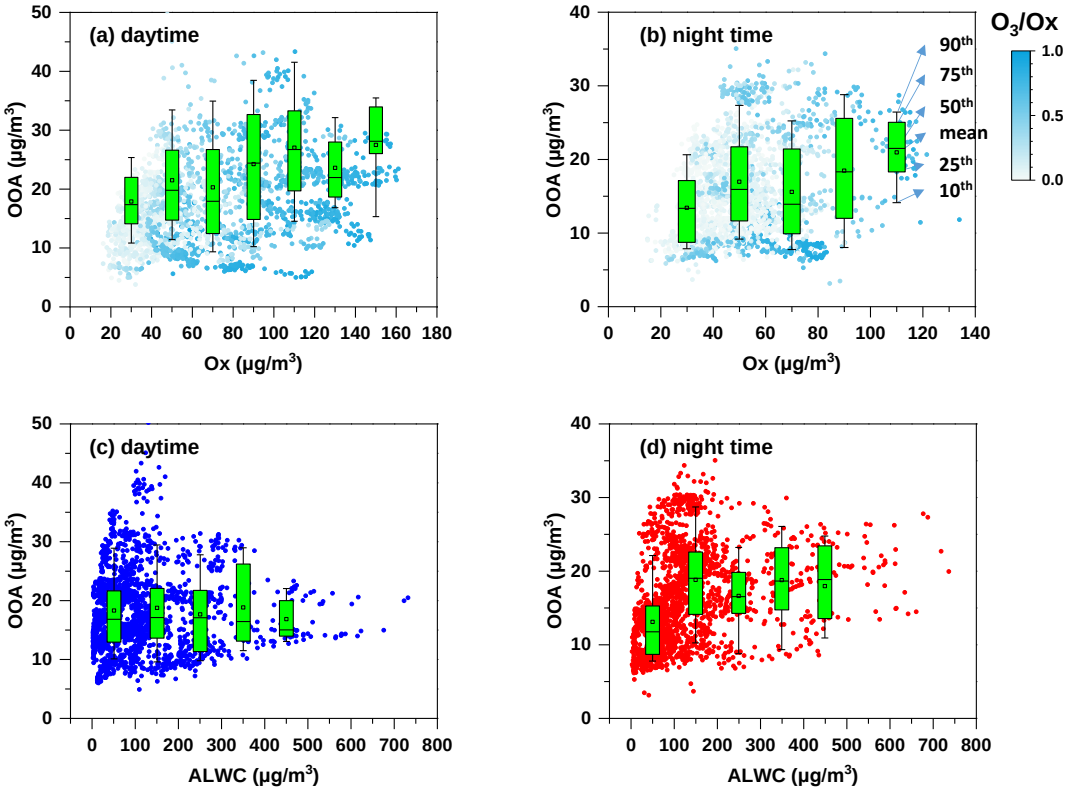

Fig. S5 OOA concentration as a function of (a) Ox and (c) ALWC during daytime. (b) and (d) are the same as (a) and (c) but during nighttime. The data of OOA concentration are grouped into different bins according to 20 μg/m^3 increment of Ox and 100 μg/m^3 increment of ALWC during both daytime and nighttime. The colour scale represents O_3/Ox ratios in (a) and (b). The mean (square), 50th (horizontal line inside the box), 25th and 75th percentiles (lower and upper box), and 10th and 90th percentiles (lower and upper whiskers) of the box chart are marked in (b).

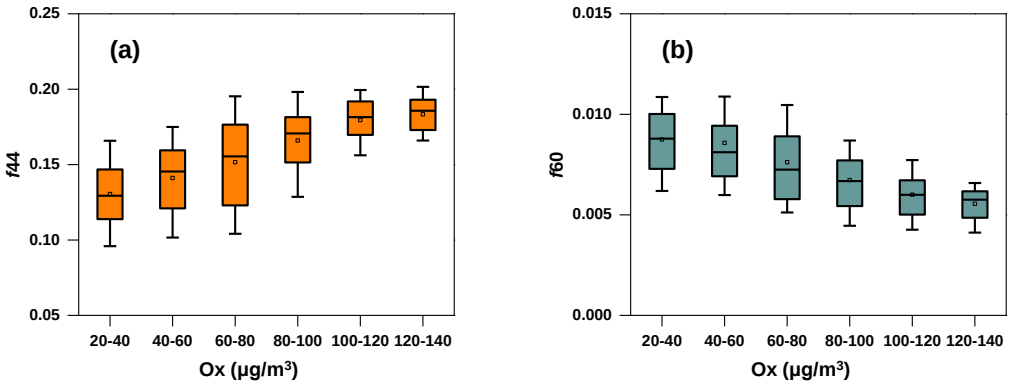

Fig. S6 Box chart of (a) *f*44 and (b) *f*60 as a function of Ox concentration. The data are grouped into different bins according to 20 μg/m^3 increment of Ox

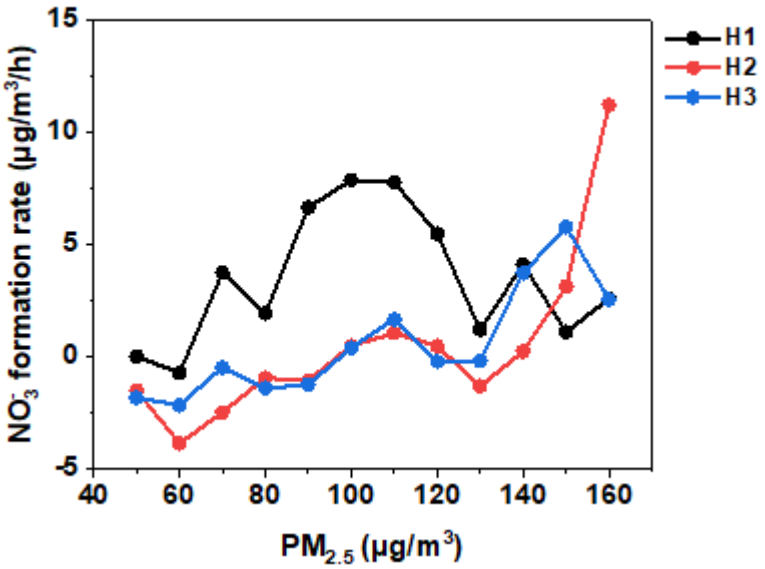

Fig. S7 Average nitrate formation rate as a function of $PM_{2.5}$ concentration during H1, H2 and H3

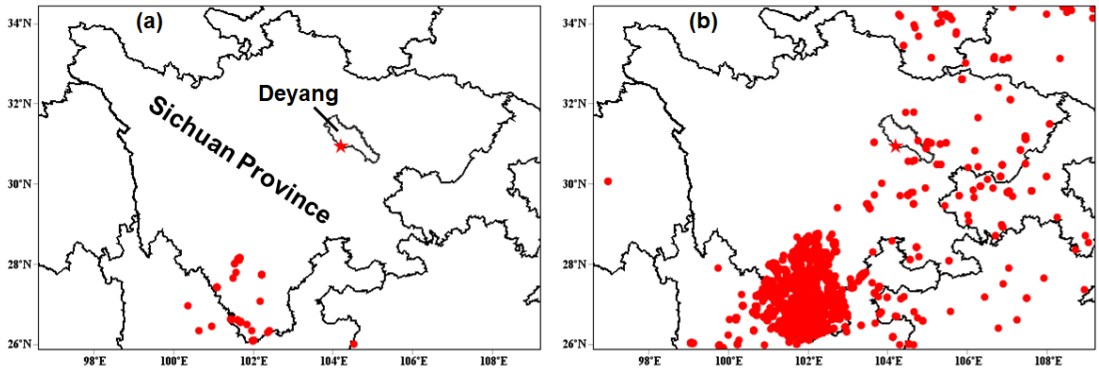

Fig. S8 Fire maps of areas around Deyang during (a) non-haze, (b) H2 and H3 periods. The Fire Maps were acquired from Fire Information for Resource Management System (FIRMS) developed by the National Aeronautics and Space Administration (NASA). The data of VIIRS (375m) was used (https://firms.modaps.eosdis.nasa.gov/active_fire/).

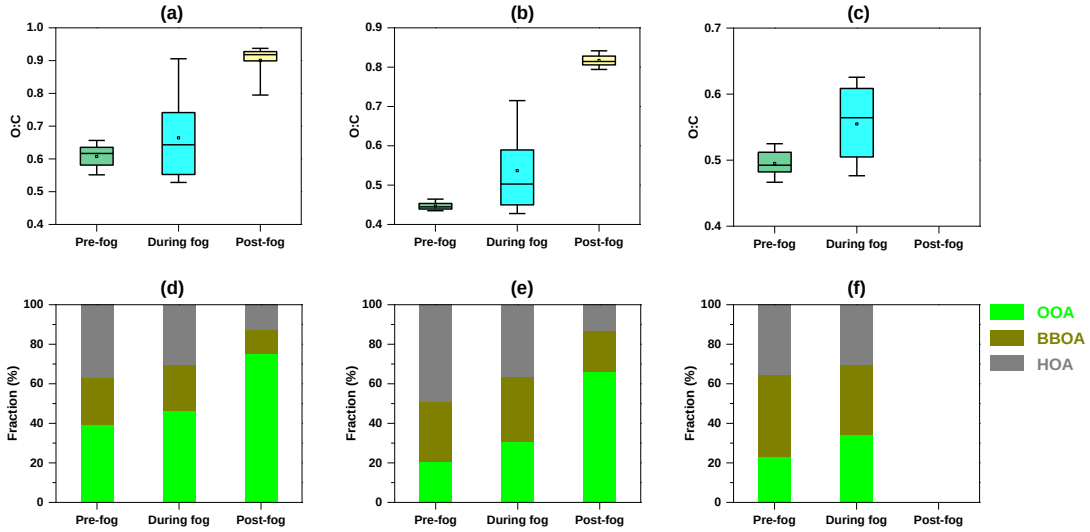

Fig. S9 Variation of O:C of OA and relative contribution of OOA, BBOA, and HOA to OA during the evolution of (a), (d) F1, (b), (e) F2, and (c), (f) F3.

Table S1 Summary of mass concentrations of $PM_{2.5}$ compositions measured during winter in different cities.

Species	This study[a]	Chengdu[b]	Chongqing[b]	Xi'an[c]	Changzhou	Beijing[d]
OA	39.2 ±3.9	N.A.	N.A.	64.2 ±40.6	31.2 ±11.9	103 ±33
NO_3^-	29 ±14	33.4 ±29.5	15.8 ±9.5	27.7 ±20.4	24.1 ±11.8	43 ±11
NH_4^+	15.1 ±6.4	12 ±7.9	11.3 ±5.2	12.5 ±9.1	13.1 ±3.7	14.9 ±5.1
SO_4^{2-}	10 ±4.2	16.6 ±13	17.5 ±7.4	17.6 ±14.2	18.7 ±7.6	47 ±15
Cl^-	5.2 ±4.1	N.A.	1.6 ±1.2	5.1 ±4.0	N.A.	35.4 ±7.9
Reference		(Huang et al., 2021)	(Wang et al., 2018)	(Duan et al., 2021)	(Ye et al., 2017)	(Elser et al., 2016)

[a] The data of rainy hours (0:00-9:00 25 December, 2021 & 0:00-8:00 1 January, 2022) were removed.

[b] The concentrations of water-soluble inorganic ions were measured by an ion chromatography, while the compositions in other cities listed in the table were measured by AMS.

[c] The concentrations of different compositions were measured before COVID-19 lockdown.

[d] The concentrations of different compositions were measured during extreme haze episodes.

Table S2 Description of the PMF solutions

Factor numbers	fpeak	Q/Qexp	Comment
2	0	3.13	Too few factors and large residuals.
3	0	2.64	**Optimum PMF solution. Q/Qexp decreases by 15.7 %. Temporal profile and diurnal variation of different factors are consistent with external tracers. The factors (HOA, BBOA, and OOA) resolved also represent major OA sources around the observation site.**
4	0	2.25	Q/Qexp decreases by 14.8 %. A new factor (factor2 in Fig. S4 (b)) with high m/z 55/ m/z 57, which makes itself look like cooking organic aerosol (COA), is separated. However, the diurnal profile of this factor does not show apparent peaks at noon and in the evening. The observation site is not affected by intense cooking emissions either.
5	0	2.03	Q/Qexp decreases by 10 %. OOA is split into two factors with similar time series. One of the factors (factor4 in Fig. S4 (c)) has too low m/z 44 signal intensity, which is not reasonable for OOA.

Table S3 Summary of meteorological parameters, mass concentrations of $PM_{2.5}$ species, OA factors and elemental ratios during different episodes.

	H1	H2	H3	F1	F2	F3	Overall
Meteorological Parameters							
T (℃)	8.2 ±2.7	6.6 ±2.8	8.0 ±2.4	6.2 ±2.3	1.5 ±3.2	4.7 ±1.3	7.3 ±2.8
RH (%)	80.7 ±11.3	81.5 ±11.7	79.7 ±12.4	99.9 ±0.3	99.0 ±1.4	99.5 ±0.7	81.0 ±12.4
WS (m/s)	0.7 ±0.5	0.7 ±0.4	0.7 ±0.4	0.9 ±0.4	0.7 ±0.2	0.6 ±0.2	0.7 ±0.5
SR (W/m^2) [a]	297 ±156	318 ±157	276 ±162	470	500	75	276 ±164
$PM_{2.5}$ species ($\mu g/m^3$)							
Org	45.6 ±18.4	42.1 ±11.5	42.2 ±11.8	53.3 ±12.8	45.0 ±12.7	45.4 ±8.4	39.2 ±15.7
NO_3^-	34.3 ±17.4	33.5 ±11.1	30.2 ±11.0	41.1 ±17.8	22.3 ±12.7	23.0 ±4.9	29.0 ±13.9
SO_4^{2-}	10.5 ±4.7	11.5 ±3.4	10.3 ±3.8	14.6 ±6.7	10.3 ±2.2	13.0 ±6.1	10.1 ±4.2
NH_4^+	16.9 ±7.6	17.1 ±5.0	15.8 ±5.5	21.3 ±8.6	15.3 ±3.8	13.6 ±2.5	15.1 ±6.4
Chl	5.8 ±3.3	5.1 ±2.8	5.9 ±4.4	8.3 ±3.6	16.2 ±10.9	8.1 ±2.7	5.2 ±4.1
BC	6.7 ±2.6	6.2 ±2.3	7.1 ±2.2	8.3 ±1.9	9.3 ±2.8	9.3 ±1.0	6.2 ±2.8
OA ($\mu g/m^3$)							
HOA	11.7 ±7.6	10.5 ±6.9	8.6 ±5.1	13.9 ±4.6	16.3 ±7.7	11.0 ±2.9	8.9 ±6.5
BBOA	7.7 ±5.5	10.0 ±4.7	10.6 ±4.6	11.2 ±3.8	14.7 ±5.2	13.0 ±3.0	8.9 ±5.4
OOA	18.3 ±7.4	20.5 ±6.9	15.5 ±4.4	22.3 ±10.1	12.8 ±5.1	12.1 ±2.7	16.3 ±6.8
Elemental ratios [b]							
O/C	0.70 ±0.14	0.71 ±0.14	0.68 ±0.12	0.66 ±0.13	0.54 ±0.13	0.55 ±0.06	0.71 ±0.14
H/C	1.54 ±0.03	1.56 ±0.02	1.58 ±0.02	1.56 ±0.01	1.59 ±0.01	1.59 ±0.01	1.56 ±0.09
$\overline{OS_c}$	-0.12 ±0.39	-0.14 ±0.28	-0.23 ±0.25	-0.23 ±0.26	-0.51 ±0.22	-0.48 ±0.12	-0.14 ±0.31

[a] The daily maximum was used for calculating the average values during different episodes

[b] The O/C and H/C were determined by the parameterization proposed by Canagaratna et al. (2015).

The $\overline{OS_c}$ was calculated as 2O/C - H/C recommended by (Heald et al., 2010).

References

Canagaratna, M. R., Jimenez, J. L., Kroll, J. H., Chen, Q., Kessler, S. H., Massoli, P., Hildebrandt Ruiz, L., Fortner, E., Williams, L. R., Wilson, K. R., Surratt, J. D., Donahue, N. M., Jayne, J. T., and Worsnop, D. R.: Elemental ratio measurements of organic compounds using aerosol mass spectrometry: characterization, improved calibration, and implications, Atmos. Chem. Phys., 15, 253-272, https://doi.org/ 10.5194/acp-15-253-2015, 2015.

Duan, J., Huang, R., Chang, Y., Zhong, H., Gu, Y., Lin, C., Hoffmann, T., and O'Dowd, C.: Measurement report of the change of PM2.5 composition during the COVID-19 lockdown in urban Xi'an: Enhanced secondary formation and oxidation, Sci. Total Environ., 791, 148126, https://doi.org/ 10.1016/j.scitotenv.2021.148126, 2021.

Elser, M., Huang, R., Wolf, R., Slowik, J. G., Wang, Q., Canonaco, F., Li, G., Bozzetti, C., Daellenbach, K. R., Huang, Y., Zhang, R., Li, Z., Cao, J., Baltensperger, U., El-Haddad, I., and Prévôt, A. S. H.: New insights into PM2.5 chemical composition and sources in two major cities in China during extreme haze events using aerosol mass spectrometry, Atmos. Chem. Phys., 16, 3207-3225, https://doi.org/ 10.5194/acp-16-3207-2016, 2016.

Heald, C. L., Kroll, J. H., Jimenez, J. L., Docherty, K. S., DeCarlo, P. F., Aiken, A. C., Chen, Q., Martin, S. T., Farmer, D. K., and Artaxo, P.: A simplified description of the evolution of organic aerosol composition in the atmosphere, Geophys. Res. Lett., 37, https://doi.org/ 10.1029/2010GL042737, 2010.

Huang, X., Zhang, J., Zhang, W., Tang, G., and Wang, Y.: Atmospheric ammonia and its effect on PM2.5 pollution in urban Chengdu, Sichuan Basin, China, Environ. Pollut., 291, 118195, https://doi.org/ 10.1016/j.envpol.2021.118195, 2021.

Wang, H., Tian, M., Chen, Y., Shi, G., Liu, Y., Yang, F., Zhang, L., Deng, L., Yu, J., Peng, C., and Cao, X.: Seasonal characteristics, formation mechanisms and source origins of PM2.5 in two megacities in Sichuan Basin, China, Atmos. Chem. Phys., 18, 865-881, https://doi.org/ 10.5194/acp-18-865-2018, 2018.

Ye, Z., Liu, J., Gu, A., Feng, F., Liu, Y., Bi, C., Xu, J., Li, L., Chen, H., Chen, Y., Dai, L., Zhou, Q., and Ge, X.: Chemical characterization of fine particulate matter in Changzhou, China, and source apportionment with offline aerosol mass spectrometry, Atmos. Chem. Phys., 17, 2573-2592, https://doi.org/ 10.5194/acp-17-2573-2017, 2017.